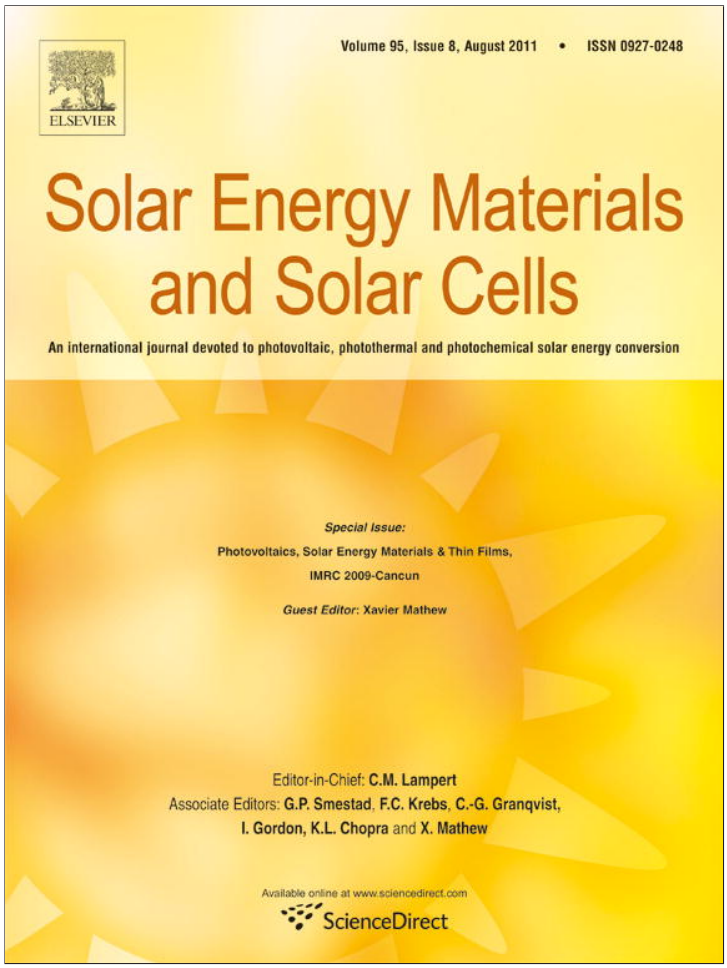

Solar Energy Materials & Solar Cells 95 (2011) 2194–2199

Contents lists available at ScienceDirect

Solar Energy Materials & Solar Cells

journal homepage: www.elsevier.com/locate/solmat

Comparison of various sol–gel derived metal oxide layers for inverted organic solar cells

Hyunchul Oh [a,c,*], Johannes Krantz [a], Ivan Litzov [a], Tobias Stubhan [a], Luigi Pinna [a,b], Christoph J. Brabec [a,b]

[a] Institute of Materials for Electronics and Energy Technology (I-MEET), Friedrich-Alexander-University of Erlangen-Nuremberg, Martensstraße 7, 91058 Erlangen, Germany
[b] Bavarian Center for Applied Energy Research (ZAE Bayern), Am Weichselgarten 7, 91058 Erlangen, Germany
[c] Max Planck Institute for Metals Research, Heisenbergstr.3, 70569 Stuttgart, Germany

ARTICLE INFO

Article history:
Received 16 January 2011
Received in revised form
8 March 2011
Accepted 14 March 2011
Available online 13 April 2011

Keywords:
Al doped ZnO (AZO)
ZnO
TiO_x
Sol–gel synthesis
Inverted Organic Solar cells
Charge selective extraction layer

ABSTRACT

Inverted bulk-heterojunction solar cells have recently captured high interest due to their environmental stability as well as compatibility to mass production. This has been enabled by the development of solution processable n-type semiconductors, mainly TiO_2 and ZnO. However, the device performance is strongly correlated to the electronic properties of the interfacial materials, and here specifically to their work function, surface states as well as conductivity and mobility. It is noteworthy to say that these properties are massively determined by the crystallinity and stoichiometry of the metal oxides. In this study, we investigated aluminum-doped zinc oxide (AZO) as charge selective extraction layer for inverted BHJ solar cells. Thin AZO films were characterized with respect to their structural, optical and electrical properties. The performance of organic solar cells with an AZO electron extraction layer (EEL) is compared to the performance of intrinsic ZnO or TiO_x EELs. We determined the transmittance, absorbance, conductivity and optical band gap of all these different metal oxides. Furthermore, we also built the correlations between doping level of AZO and device performance, and between annealing temperature of AZO and device performance.

1. Introduction

Bulk-heterojunction (BHJ) organic solar cells have attracted considerable attention in the past few years owing to their potential of providing environmentally safe, flexible, lightweight and inexpensive solar cells. However, their longevity and a relatively low power conversion efficiency compared to inorganic solar cells have been the major limitations for faster commercialization.

Normal geometry BHJ organic solar cells can suffer from degradation of the top electrode, which is normally made of a low-work-function metal that is reactive and oxidized easily in air [1]. The inverted device geometry is an attractive concept to improve the longevity, because it only uses electrode and interface materials with a higher work function and significantly improved air stability. For efficient inverted BHJ solar cells, transparent and conductive interfacial materials, which are inserted between transparent conductive electrode and photoactive layer, are required. The role of this electron extraction layers is not only to form an electron selective layer but also to form an electrical contact to a less air sensitive high work function metal, e.g. Ag or Au.

Recently a thin layer (10–20 nm) of solution-processed sol–gel titanium oxide [2–4] or zinc oxide [5–8] has been successfully applied as an interfacial layer in the normal and inverted geometry [6,9–13]. These materials are transparent in the visible light spectrum but absorb ultraviolet (UV) light. The layer thicknesses are also tunable without absorption loss in the visible light spectrum [14]. In order to improve the power conversion efficiency (PCE) the thickness of the interfacial layer was frequently decreased to reduce serial resistance losses. In mass production based on printing technologies, however, very thin interfacial layers are critical due to low mechanical robustness. Further, very thin interfacial layers may have reduced protective properties against chemical or physical reaction between the active layer and the electrode.

One way to overcome these limitations is the use of doped materials, e.g. aluminum-doped zinc oxide, and to process thick layers. By that, an increase in the layer thickness would not result in a serial resistance increase. Numerous ways of doping ZnO were suggested in the literature [15–21]. Recently, Krebs et al. introduced the aluminum-doped zinc oxide (AZO) as an interfacial layer in organic solar cells produced by a sol–gel method [22,23]. However, they did not describe any of AZO film effects and device performance on organic solar cells. In order to obtain an optimal AZO interfacial layer for organic solar cell, characterization and performance of AZO film in organic solar cells have to be investigated, but this has not

* Corresponding author. Tel.: +49 (0)711 689 1800; fax: +49 (0)711 689 1952.
E-mail address: oh@mf.mpg.de (H. Oh).

0927-0248/$ - see front matter © 2011 Elsevier B.V. All rights reserved.
doi:10.1016/j.solmat.2011.03.023

been published yet. The lack of interest in this matter was probably due to the requirement for a high temperature post treatment, which is unsuitable for flexible substrates. Also, the difficulties in doping Al into nano-sized ZnO crystalline produced by sol–gel method, the so-called 'self-purification', makes this approach less attractive [24].

In this study, we investigated solution-processed aluminum-doped zinc oxide (AZO) as charge selective extraction layer for inverted BHJ solar cells. Thin AZO films were characterized with respect to their structural, optical and electrical properties. The performance of solar cells with an AZO electron extraction layer is compared with that consisting of an intrinsic ZnO or TiO_x layer. We determined the transmittance, absorbance, conductivity and optical band gap of all these different metal oxides. Furthermore ZnO nanoparticles with various aluminum doping concentrations were processed under relatively low annealing temperatures. Sufficient conductivity for use as EEL in organic solar cells was already found for annealing temperatures as low as 260 °C.

2. Experimental methods

2.1. Materials synthesis

ZnO synthesis: The wet chemical synthesis of ZnO nanoparticles was performed using the method outlined by Harranck et al. [25]. Namely, it was done in methanol via hydroxylation of zinc acetate dihydrate ($ZnAc \cdot 2H_2O$) by potassium hydroxide (KOH). The solution of 1.48 g of potassium hydroxide (KOH) in 65 ml of methanol was prepared by stirring it with a magnetic bar for about 30 min. Then, 2.95 g of zinc acetate dihydrate ($ZnAc \cdot 2H_2O$) were dissolved in 125 ml of methanol at 65 °C for 10 min with a stirring speed of 400 rpm. After that potassium hydroxide (KOH) solution was added to the zinc acetate dihydrate ($ZnAc \cdot 2H_2O$) solution while continuously being stirred. After 150 min of reaction at 65 °C the solution was cooled down over night to precipitate the solute. The samples were then washed for 20 and twice for 10 min at 23 °C via centrifugation at 4000 rpm. Finally, the ZnO nanoparticles in white powder form were suspended in various solvents such as acetone, ethanol and isopropanol while being stirred at a speed of 300 rpm for a week, leading to a transparent suspension.

TiO_x synthesis: TiO_x nanoparticles were synthesized by modifying the method used by Wang et al. [26]. 0.5 ml of titanium chloride ($TiCl_4$) was added slowly to 2 ml of ethanol and then mixed in 10 ml of anhydrous benzyl alcohol ($C_6H_5CH_2OH$), which forms a yellow solution. After 9 h of reaction at 80 °C, the solution was cooled down over night to precipitate the solute. 1 ml of the resulting suspension was precipitated in 12 ml of diethyl ether and centrifuged for 20 and twice for 10 min at 23 °C at 5000 rpm to isolate the nanoparticles from the solvent and the unreacted precursor. The TiO_x nanoparticle precipitate was suspended in acetone and ethanol, resulting in a transparent sol of nanocrystals.

Al doped ZnO (AZO) synthesis: Al doped ZnO using ethanol solvent was synthesized by modifying a technique outlined by Alam and Cameron. [27]. 2.2 g of Zinc acetate ($ZnAc \cdot 2H_2O$) and 0.016 g (1 at%) of aluminum hydroxide acetate ($HOAl(C_2H_3O_2)_2$) were mixed together and dissolved in 100 ml of ethanol. The solution was refluxed at 80 °C for 3 h at a stirring speed of 450 rpm to get a transparent solution. In order to stabilize the Al doped ZnO complex, 0.61 ml of monoethanolamine (MEA) was added to AZO suspension. The molar ratio of MEA to zinc acetate ($ZnAc \cdot 2H_2O$) was maintained at 1.0 and the concentration of zinc acetate was 0.10 mole. The coated substrates were heated at 260 °C for 10 min in air.

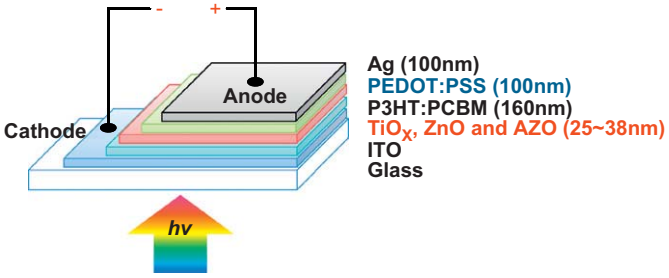

Fig. 1. Scheme of Inverted Organic Solar Cells.

2.2. Characterization of materials and device fabrication

Characterization: The crystal structure of ZnO, TiO_x and AZO films was identified by X-ray diffractometer (XRD) using CuKα radiation. The optical properties such as transmittance and absorbance spectra were evaluated using an UV–vis–NIR spectrometer (Perkin–Lambda 950). The electrical conductivity was measured by a 4 point layout with a potentiostat (Autolab, Metrohm). The thicknesses of the thin films were measured by an interferometer (NanoFocus).

Device Fabrication: Fig. 1 shows inverted geometry organic solar cells. The inverted organic solar cell comprises of an active layer of P3HT:PCBM blend sandwiched between a transparent conductive oxide (TCO) coated glass as a cathode and a top metal layer as an anode. ITO glasses with and without ZnO, TiO_x and Al doped ZnO (AZO) electron extraction layers were used for the fabrication of the inverted organic solar cells under identical processing conditions. P3HT:PCBM (ratio 1:1) active layer were doctor-bladed in air from blend solution in chlorobenzene at a speed of 20 mm/s and a temperature of 60 °C on the surface of the various n-type metal oxide coated substrates. The resulting active layer thickness was about 160 nm. A thin layer of PEDOT:PSS was doctor-bladed at a speed of 60 mm/s and a temperature of 60 °C, which resulted in a 100 nm thick layer. Then the device was annealed in inert atmosphere on a hotplate at 140 °C for 10 min. Next, an Ag layer (~100 nm) was thermally evaporated on the PEDOT:PSS surface at $\sim 1*10^{-6}$ mbar through a shadow mask to define an active area of 10.4 mm^2. The current density–voltage (J–V) characteristics were measured with a source measurement unit from BoTest. For illumination, an Oriel Sol 1A solar simulator calibrated with a silicon-based reference cell was used providing an AM 1.5 G spectra at 100 mW/cm^2 without any further corrections.

3. Results and discussion

3.1. Characterization of ZnO, TiO_x and AZO

The structure of ZnO, TiO_x and AZO nanoparticles was measured using X-Ray diffraction (XRD) by a CuKα source at an angle ranging from 20° to 80° by step-scanning with a step size of 0.02°. The as-coated films on glass were amorphous, but after drying in air, wurtzite and ZnO anatase TiO_x was found (Fig. 2(a) and (b)). Fig. 2(c) shows a comparison of the X-ray diffraction pattern of a 1 at% doped AZO with that of an intrinsic ZnO layer. It is well-known that AZO thin films are highly textured with the c-axis perpendicular to the substrate surface, especially in the (0 0 2) orientation. This (0 0 2) preferred orientation is due to the minimal surface energy, which the hexagonal structure (c-plane to the ZnO crystallites) corresponds to the densest packed plane [28–30]. If Al^{3+} ions only substitute Zn^{2+} ions, the lattice parameter of AZO crystals decreases and the (0 0 2) peak shifts to higher 2θ value due to the smaller radius of Al^{3+} ions (0.53 Å) compared to Zn^{2+} ions (0.75 Å) [28].

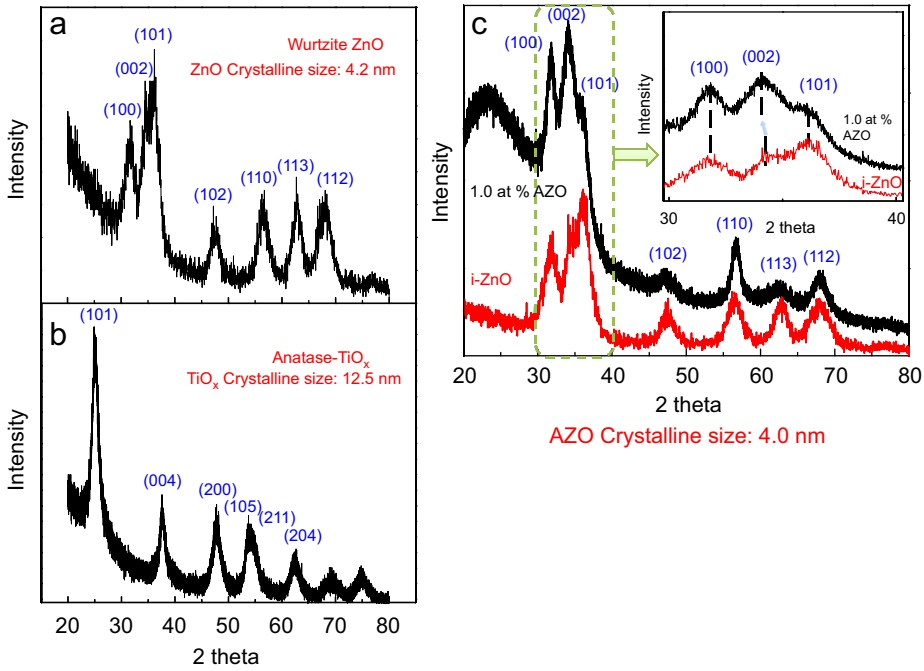

Fig. 2. X-ray diffraction pattern of (a) ZnO, (b) TiO_x and (c) XRD comparison between AZO and ZnO films. The base-line at low angles of the XRD pattern is not flat since a glass substrate was used.

Table 1
Comparison of (0 0 2) diffraction peak position.

Plane	ZnO	AZO	**Difference**
100	31.87	31.85	**−0.02**
002	34.79	34.20	**−0.59**
101	36.25	36.15	**0.10**

Table 2
Conductivity measurement of all electron extraction layers.

Samples	**Conductivity (S/cm)**
ZnO in acetone	2.22E−06
ZnO in EtOH	1.63E−06
ZnO in IPA	5.34E−06
TiOx in EtOH	4.50E−04
0.5 at% AZO_EtOH at 260 °C	2.12E−03
1.0 at% AZO_EtOH at 260 °C	2.35E−03
2.0 at% AZO_EtOH at 260 °C	2.06E−03
1.0 at% AZO_EtOH at 200 °C	2.43E−05
1.0 at% AZO_EtOH at 150 °C	8.86E−07

However, since our ZnO particles are of nanometer dimension, i.e. in the order of the Bohr radius or even smaller, direct substitution Zn^{2+} ions by Al^{3+} ions is unlikely [24]. Thus our results indicate that Al^{3+} ions are found at interstitional sites, resulting in an increased lattice parameter of AZO crystals. The peak position of AZO diffraction pattern of (0 0 2) plane is shifted towards a lower 2θ value as listed in Table 1. Broadening of each XRD peak reveals the nanocrystalline nature of the ZnO nanoparticles. Crystalline sizes (D) of the ZnO, TiO_x and AZO nanoparticles were calculated using the Scherrer formula [31]

$$D = 0.9\lambda/(\beta\cos\theta) \tag{3.1}$$

where λ is the wavelength of the X-rays (λ=0.154 nm), β is the full width in radians at half-maximum of the diffraction peaks (FWHM) and θ is the Bragg angle of the X-ray pattern. The calculated mean crystalline size D of ZnO, AZO and TiO_x was 4.2, 4.0 and 12.5 nm, respectively.

Thin layers from the three MeO_x were characterized by conductivity and absorption measurements. The conductivity data is listed in Table 2. Interestingly, we observe a fairly high conductivity of the TiOx films and a fairly low conductivity of the ZnO films. The low conductivity of the ZnO films may be explained by the presence of oxygen molecules near the ZnO surface. These oxygen molecules can capture free electrons from the ZnO, which were otherwise created by stoichiometric oxygen defects. As a consequence, the conductivity of the ZnO is decreased [32]. Alternatively, a good 1:1 stoichiometry would also result in low conductive ZnO. Given the small size of our nanoparticles, we speculate that the first mechanism is more relevant for our ZnO. The highest conductivity was found for AZO, as a function of the doping rate and annealing temperature (Table 2). The dependence of the conductivity on the doping ratio is rather weak. Conductivity increases from 2.12×10^{-3} to 2.35×10^{-3} S/cm with an increase in the Al concentration from 0.5 to 1.0 at%, and then drops to 2.06×10^{-3} S/cm at 2.0 at%. Such trends are not unusual and are frequently interpreted as a neutralization of the dopant atom [17,27–30,33]. The annealing temperature has a much stronger influence on the conductivity due to recrystallization of the films. Therefore, the poor crystallinity of the films annealed at a low temperature (150 °C) results in relatively poor conductivity.

The optical transmittance spectra of the TiO_x, ZnO and AZO films are presented in Fig. 3. In all cases the films were found to be transparent (over 95%) in the visible range with a sharp absorption edge at wavelengths of around 385 nm for AZO, 375 nm for ZnO and 350 nm for TiO_x. The optical absorption coefficient of a direct band gap semiconductor near the band edge is given by [34]

$$ahv = A(hv - Eg)^{1/2} \tag{3.2}$$

where A is the proportionality constant. By plotting $(\alpha hv)^2$ against hv, Eg can be found by extrapolating the linear portion of the curve to

zero absorption. The calculated mean optical band gap was 3.34 eV for AZO, 3.44 eV for ZnO and 3.85 eV for TiO_x, as shown in Fig. 4.

The relevant data for the three metal oxides are summarized in Table 3. Table 3 presents the details of the individual synthesis reactions, the used solvents, the film thickness, crystalline size, surface roughness and optical band gap for TiO_x, ZnO and Al doped ZnO thin layers. All listed film thicknesses are in the range 25–40 nm.

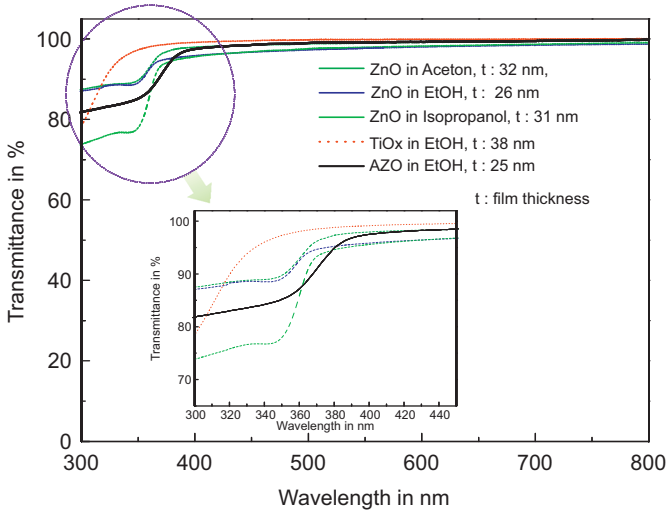

Fig. 3. Transmittance comparison of ZnO, TiO_x and AZO films.

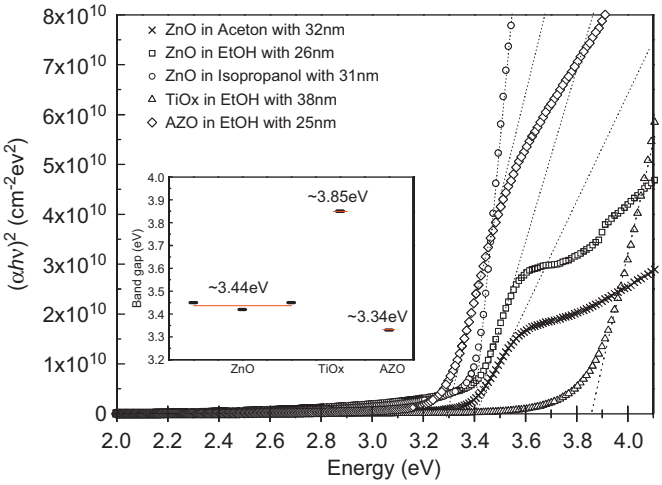

Fig. 4. Plot of $(\alpha h\nu)^2$ vs. photon energy $h\nu$ for ZnO, TiO_x and AZO films.

3.2. Fabrication of inverted organic solar cell

The *J–V* curves of the devices are shown in Fig. 5 and the extracted device parameters are summarized in Table 4. Overall, we noticed that all devices suffer from a rather strong photo-shunt, independent of the interface layer material, which limits the *FF* to values of less than 60%.

First, we investigated to determine the preferable solvent for the i-ZnO and TiO_x interfacial layer, shown as inset in Fig. 5. None of these interfacial layers is fully optimized with respect to layer thickness, surface roughness and semiconductor thickness. The variations in non-optimized device performance are not significant in terms of open-circuit voltage (V_{oc}) as shown in Table 4. However, on the average it was found that that ZnO in acetone and TiO_x in EtOH have slightly better device performance than

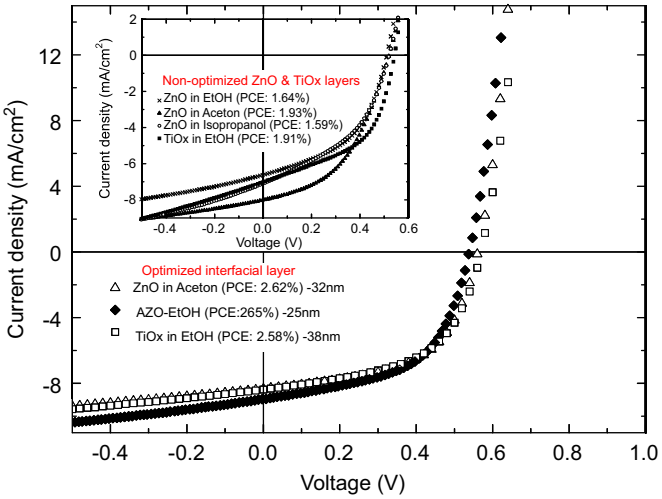

Fig. 5. Inverted Organic Solar Cells: *J–V* characteristics of devices with optimized ZnO, TiO_x and AZO films under simulated solar irradiation of AM 1.5 G. Non-optimized ZnO and TiO_x with various solvent are inset to determine the most suitable solvent for ZnO and TiO_x.

Table 4
Inverted Organic Solar Cells: *J–V* characteristics of devices with various interfacial layers.

	V_{oc} (mV)	J_{sc} (mA/cm²)	*FF* (%)	PCE (%)
ZnO in EtOH (non-optimized)	0.51	6.63	48.5	1.64
ZnO in Acetone (non-optimized)	0.52	8.02	46.3	1.93
ZnO in IPA (non-optimized)	0.52	7.11	43.0	1.59
ZnO in Acetone (Optimized)	**0.56**	**8.33**	**56.5**	**2.62**
TiO_x in EtOH (non-optimized)	0.54	7.02	50.5	1.91
TiO_x in EtOH (Optimized)	**0.57**	**8.38**	**54.4**	**2.58**
1 at% AZO-EtOH at 260 °C	**0.54**	**8.97**	**55.0**	**2.65**

Table 3
Summary of all electron extraction layer properties produced by sol–gel method.

	ZnO in acetone	ZnO in EtOH	ZnO in IPA	1 at% AZO with EtOH	TiO_x in EtOH
Reaction	ZnAc+KOH+MeOH			ZnAc+AlAc+EtOH	$TiCl_4$+EtOH+Anhydrous benzyl alcohol
Dispersion Solvent	Acetone	EtOH	IPA	–	EtOH
Concentration (mg/ml)	20	10	20	–	30
Stabilizer	–	–	–	MEA	–
Thickness (nm)	32	26	31	25	38
Crystalline size (nm)	4.2	4.0	12.5		
Surface Roughness (nm)	3.7	11.3	11.5	2.5	2.3
Band gap (eV)	3.45	3.42	3.45	3.34	3.85
Annealing	–	–	–	260 °C for 10min	–

ZnO in EtOH or isopropanol. Although the inset in Fig. 5 suggests some variations in the short-circuit current density (J_{sc}), we rather believe this as a statistical variation than a trend. Therefore, large variation in the power conversion efficiency for the non-optimized i-ZnO and TiO_x layer is mainly due to the *FF*, which seems to be influenced by the different processing conditions and solvents of these layers. Compared to that, the device performance of Al doped ZnO layers shows less scattering and, on the average, we find better fill factors. After further optimization of the layer quality of ZnO in acetone and TiO_x in ethanol, the power conversion efficiency achieved around 2.5%, which results in comparable device performance with Al-doped ZnO as shown in Fig. 5. This first data indicates that solution-processed AZO layers have at least the same performance potential as i-ZnO or TiO_x interfacial layers. In order to study the effect of aluminum concentration on the device properties, different values of dopant concentrations (0.5, 1.0 and 2.0 at%) were used. The *J–V* characteristics of the inverted device as a function of doping concentration are plotted in Fig. 6. Again, we notice a rather strong photoshunt, which is independent of the doping ratio. In good agreement with the previous data, we observe little variation in the open-circuit voltage (V_{oc}), and rather small variation in the *FF* and short-circuit current density (J_{sc}) as a function of the doping degree. From the data it is safe to conclude, that a variation of the doping degree between 0.5% and 2% does not make a major impact on the device performance.

In organic solar cell applications, the processing temperature is one of the more critical parameters. This is currently the biggest limitation of the AZO layers since fully functional AZO films still require an annealing recrystallization step of over 250 °C to show best performance. We therefore investigated the annealing temperature dependence of AZO films. The *J–V* characteristics of inverted devices as a function of annealing temperature are plotted in Fig. 7. Similarly, the variation of V_{oc} in the device performance is not significant. The J_{sc} and *FF* at the annealing temperatures of 200 °C and 260 °C remained quite constant, resulting in comparable device performance. However, an annealing temperature of 150 °C resulted in poorer J_{sc}. AZO films annealed at 150 °C have conductivity in the order of 10^{-6} S/cm (see Table 2). Such low conducting interface layers will result in a R_s increase, even for layer thicknesses of 30 nm or less. The measured device parameters for different doping concentrations and annealing temperatures are summarized in Table 5. In summary, these data indicate that that a low temperature process for AZO is not out of the world.

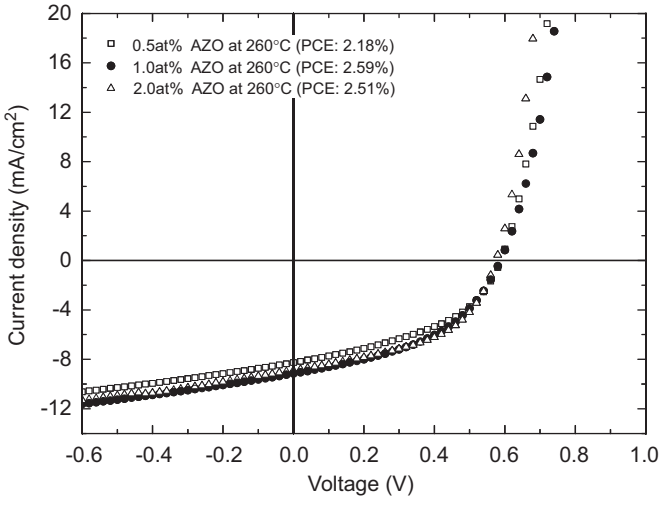

Fig. 6. Inverted Organic Solar Cells: *J–V* characteristics of devices dependence on Al doping concentration.

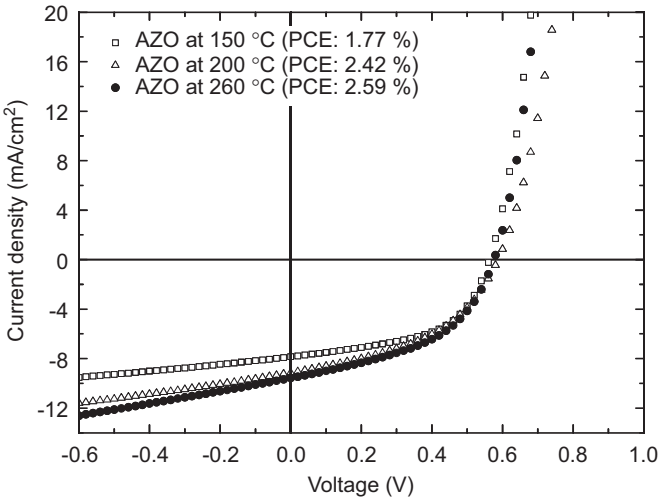

Fig. 7. Inverted Organic Solar Cells: *J–V* characteristics of devices dependence on annealing temperature.

Table 5
Performance of organic solar cells with an AZO electron injection layer dependence on doping concentration and annealing temperature.

	Voc(mV)	Jsc(mA/cm²)	FF(%)	PCE(%)
0.5 a.t% AZO at 260°C [a]	0.58	8.26	45.1	2.18
2.0 at.% AZO at 260°C [a]	0.57	8.90	49.4	2.51
1.0 at.% AZO at 260°C [a], [b]	0.57	9.57	47.7	2.59
1.0 at.% AZO at 200°C [b]	0.59	9.14	44.9	2.42
1.0 at.% AZO at 150°C [b]	0.57	7.02	43.0	1.77

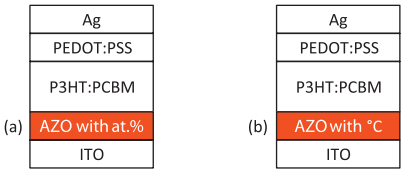

4. Conclusions

In conclusion, we compared various electron extraction layers and compared their impact on the performance of inverted organic solar cells (Substrate/ITO/ZnO, TiO_x or AZO/P3HT:PCBM/PETDOT:PSS/Ag). From our experiments, acetone and ethanol were good solvents for ZnO and TiO_x suspensions, respectively. The power conversion efficiency for optimized i-ZnO suspended in acetone was 2.62% (V_{oc}: 0.56 mV, J_{sc}: 8.33 mA/cm^2 and *FF*: 56.5%) while the one recorded for optimized TiO_x suspended in ethanol was 2.58% (V_{oc}: 0.57 mV, J_{sc}: 8.38 mA/cm^2 and *FF*: 54.4%). On the average, we found at least equal if not even better performance for solution-processed AZO interface layers. Furthermore, we demonstrated the effect of Al doping concentration and annealing temperature of AZO on the device performance of the solar cell. In terms of power conversion efficiency, the most suitable Al concentration was 1.0 at% and annealing temperature of AZO film was 260 °C. However, annealing temperature of AZO film at 200 °C demonstrated comparable device performance to the one annealed at 260 °C. The power conversion efficiency of 1 at% AZO annealed at 260 °C was 2.59% (V_{oc}: 0.57 mV, J_{sc}:

9.57 mA/cm^2 and *FF*: 47.7%) and of 1 at% AZO annealed at 200 °C was 2.42% (V_{oc}: 0.59 mV, J_{sc}: 9.14 mA/cm^2 and *FF*: 44.9%). The device performance of 1 at% Al doped ZnO annealed at 260 °C was the best among all samples considered for solar cell applications. For industrial applications involving roll to roll printing of solar cells on polyester, a conversion temperature above 140 °C is critical. As such, our current route towards AZO, requiring a relatively high annealing temperature (above 200 °C), for best performance is most suitable for glass based applications. Nevertheless, we are also foreseeing opportunities to further reduce the annealing temperature to values beneath 150 °C while still getting significantly higher conductivities than for intrinsic ZnO. Various concepts, including nanoparticle–sol–gel blends are currently under investigation.

The significantly higher conductivity of AZO layers does suggest that this electron extraction layer can be made much thicker than layers from i-ZnO or TiO_x. Results on the thickness dependence will be discussed in a separate manuscript [35]. We believe that this sol–gel derived AZO film as an electron extraction layer is a promising candidate for air-stable, low temperature processed inverted organic solar cells that are important for developing low-cost, large area, roll-to-roll printable solar cells.

References

[1] S.E. Shaheen, M.S. White, D.C. Olson, N. Kopidakis, D.S. Ginley, Inverted bulk-heterojunction plastic solar cells, SPIE/Newsroom (2007), doi:10.1117/2.1200704.0756.

[2] J.Y. Kim, S.H. Kim, H.H. Lee, K. Lee, W. Ma, X. Gong, A.J. Heeger, New architecture for high-efficiency polymer photovoltaic cells using solution-based titanium oxide as an optical spacer, Adv. Mater. 18 (2006) 572–576.

[3] T. Kuwabara, H. Sugiyama, T. Yamaguchi, K. Takahashi, Inverted type bulk-heterojunction organic solar cell using electrodeposited titanium oxide thin films as electron collector electrode, Thin Solid Films 517 (2009) 3766–3769.

[4] M.H. Park, J.H. Li, A. Kumar, G. Li, Y. Yang, Doping of the metal oxide nanostructure and its influence in organic electronics, Adv. Funct. Mater. 19 (2009) 1241–1246.

[5] H.-L. Yip, S.K. Hau, N.S. Baek, A.K.-Y. Jen, Polymer solar cells that use self-assembled-monolayer-modified ZnO/metals as cathodes, Adv. Mater. 20 (2008) 2376–2382.

[6] M.S. White, D.C. Olson, S.E. Shaheen, N. Kopidakis, D.S. Ginley, Inverted bulk-heterojunction organic photovoltaic device using a solution-derived ZnO underlayer, Appl. Phys. Lett. 89 (2006) 143517.

[7] A.K.K. Kyaw, X.W. Sun, C.Y. Jiang, G.Q. Lo, D.W. Zhao, D.L. Kwong, An inverted organic solar cell employing a sol–gel derived ZnO electron selective layer and thermal evaporated MoO3 hole selective layer, Appl. Phys. Lett. 93 (2008) 221107.

[8] S.K. Hau, H.-L. Yip, N.S. Baek, J. Zou, K. O'Malley, A.K.-Y. Jen, Air-stable inverted flexible polymer solar cells using zinc oxide nanoparticles as an electron selective layer, Appl. Phys. Lett. 92 (2008) 253301.

[9] A. Hayakawa, O. Yoshikawa, T. Fujieda, K. Uehara, S. Yoshikawa, High performance polythiophene/fullerene bulk-heterojunction solar cell with a TiO_x hole blocking layer, Appl. Phys. Lett. 90 (2007) 163517.

[10] K. Lee, J.Y. Kim, H. Park, S.H. Kim, S. Cho, A.J. Heeger, Air-Stable polymer electronic devices, Adv. Mater. 19 (2007) 2445–2449.

[11] H.-L. Yip, S.K. Hau, N.S. Baek, A.K.-Y. Jen, Self-assembled monolayer modified ZnO/metal bilayer cathodes for polymer/fullerene bulk-heterojunction solar cells, Appl. Phys. Lett. 92 (2008) 193313.

[12] D.C. Olson, J. Piris, R.T. Collins, S.E. Shaheen, D.S. Ginley, Hybrid photovoltaic devices of polymer and ZnO nanofiber composites, Thin Solid Films 496 (2006) 26–29.

[13] W.J.E. Beek, M.M. Wienk, M. Kemerink, X. Yang, R.A.J. Janssen, Hybrid zinc oxide conjugated polymer bulk heterojunction solar cells, J. Phys. Chem. B 109 (2005) 9505–9516.

[14] R. Steim, F.R. Koglera, C.J. Brabec, Interface materials for organic solar cells, J. Mater. Chem. 20 (2010) 2499–2512.

[15] Z. Zhao, R. Tekib, N. Koratkarc, H. Efstathiadis, P. Haldar, Metal oxide buffer layer for improving performance of polymer solar cells, Appl. Surf. Sci. 256 (2010) 6053–6056.

[16] M. Sharma, R.M. Mehra, Sol–gel derived zinc oxide films alloyed with cobalt and aluminium, Thin Solid Films 518 (2010) 3725–3730.

[17] S. Mridha, D. Basak, Aluminium doped ZnO films: electrical, optical and photoresponse studies, J. Phys. D: Appl. Phys. 40 (2007) 6902–6907.

[18] C.E. Benouisa, M. Benhalilibaa, A.S. Juarezb, M.S. Aidac, F. Chamid, F. Yakuphanoglue, The effect of indium doping on structural, electrical conductivity, photoconductivity and density of states properties of ZnO films, J. Alloys Compd. 490 (2010) 62–67.

[19] M. Caglar, Y. Caglar, S. Aksoy, S. Ilican, Temperature dependence of the optical band gap and electrical conductivity of sol–gel derived undoped and Li-doped ZnO films, Appl. Surf. Sci. 256 (2010) 4966–4971.

[20] C.-Y. Tsay, H.-C. Cheng, Y.T. Tung, W.H. Tuan, C.-K. Lin, Effect of Sn-doped on microstructural and optical properties of ZnO thin films deposited by sol–gel method, Thin Solid Films 517 (2008) 1032–1036.

[21] K. Lin, P. Tsai, Parametric study on preparation and characterization of ZnO:Al films by sol–gel method for solar cells, Mater. Sci. Eng. B 139 (2007) 81–87.

[22] J. Alstrup, M. Jørgensen, A.J. Medford, F.C. Krebs, Ultra-Fast and parsimonious materials screening for polymer solar cells using differentially pumped slot-die coating, ACS Appl. Mater. Interfaces 2 (2010) 2819–2827.

[23] R. Søndergaard, M. Helgesen, M. Jørgensen, F.C. Krebs, Fabrication of polymer solar cells using aqueous processing for all layers including the metal back electrode, Adv. Energy Mater. 1 (2011) 68–71.

[24] M. Shim, P. Guyot-Sionnest, n-type colloidal semiconductor nanocrystals, Nature 407 (2000) 981–983.

[25] O. Harnack, C. Pacholski, H. Weller, A. Yasuda, J.M. Wessels, Rectifying behavior of electrically aligned ZnO nanorods, Nano Lett. 3 (2003) 1097–1101.

[26] J. Wang, J. Polleux, J. Lim, B. Dunn, Pseudocapacitive contributions to electrochemical energy storage in TiO_2 (Anatase) nanoparticles, J. Phys. Chem. C 111 (2007) 14925–14931.

[27] M.J. Alam, D.C. Cameron, Preparation and properties of transparent conductive aluminum-doped zinc oxide thin films by sol–gel process, J. Vac. Sci. Technol. A 19 (2001) 1642–1646.

[28] S.-Y. Kuo, K.-C. Liu, F.-I. Lai, J.-F. Yang, W.-C. Chen, M.-Y. Hsieh, H.-I. Lin, W.-T. Lin, Effects of RF power on the structural, optical and electrical properties of Al-doped zinc oxide films, Microelectron. Reliab. 50 (2010) 730–733.

[29] K.H. Kim, R.A. Wibowo, B. Munir, Properties of Al-doped ZnO thin film sputtered from powder compacted target, Mater. Lett. 60 (2006) 1931–1935.

[30] W. Yang, Z. Liu, D.-L. Peng, F. Zhang, H. Huang, Y. Xie, Z. Wu, Room-temperature deposition of transparent conducting Al doped ZnO films by RF magnetron sputtering method, Appl. Surf. Sci. 255 (2009) 5669–5673.

[31] A.R. West, Effect of crystal size on the powder pattern-particle size measurement, Solid State Chemistry and Its Applications, John Wiley & Sons, New York, 1984, pp 173–175 (Chapter 5.6.5).

[32] F. Verbakel, S.C.J. Meskers, R.A.J. Janssen, Electronic memory effects in diodes of zinc oxide nanoparticles in a matrix of polystyrene or poly(3-hexylthiophene), J. Appl. Phys. 102 (2007) 083701.

[33] S.B. Majumder, M. Jain, P.S. Dobal, R.S. Katiyar, Investigations on solution derived aluminium doped zinc oxide thin films, Mater. Sci. Eng. B103 (2003) 16–25.

[34] J. Tauc, R. Grigorovici, A. Vancu, Optical properties and electronic structure of amorphous germanium, Phys. Status Solidi (b) 15 (1966) 627–637.

[35] T. Stubhan, H. Oh, L. Pinna, J. Krantz, I. Litzov, C.J. Brabec, submitted.